Exciton transport in molecular aggregates probed by time and frequency gated optical spectroscopy

Vladimir Chernyak, Tatsuya Minami, and Shaul Mukamel
Department of Chemistry, University of Rochester, Rochester, New York 14627

(Received 22 September 1999; accepted 15 February 2000)

The signatures of exciton relaxation in time-resolved fluorescence spectroscopy of molecular aggregates excited by a short pulse are expressed as an overlap of a Doorway wavepacket representing the exciton density matrix with a Window wavepacket which describes the time and frequency resolved detection. Transport and relaxation of the excitons are accounted for using the Redfield equations for the density matrix, and the complete temporal and spectral profiles of the excitation pulse and detection gate are incorporated using Wigner spectrograms. The spread in the off diagonal elements of the density matrix in the chromophore (real space) representation provides a natural measure of the relevant exciton coherence size. © *2000 American Institute of Physics.* [S0021-9606(00)00518-3]

I. INTRODUCTION

Exciton transport plays an important role in the photoinduced dynamics of molecular aggregates,[1] crystals[2,3] and superlattices.[4] Extensive recent activity had focused on *J* aggregates of cyanine dyes,[1,5–11] photosynthetic antenna complexes,[12–22] and conjugated systems with localized optical excitations, e.g., phenylacetylene dendrimers.[23,24] Despite the relatively simple structure of electronic excitations, photoinduced dynamics in molecular aggregates shows a complex interplay of strong vibronic coupling, the broad distribution of time scales of nuclear motions, and static disorder.

Computing the coupled exciton–phonon dynamics on the microscopic level constitutes a formidable task since it involves solving dynamical equations for wavepackets that are matrices in the exciton space and depend on a large number of intramolecular and solvent vibrational coordinates.[25] The relevant variable phase space can be, however, substantially reduced when separation of time scales exists between different types of motions. Faster degrees of freedom can be eliminated and incorporated through relaxation kernels for the slow variables that should be treated explicitly. A theoretical description of aggregate photodynamics starts, therefore, by determining the relevant set of slow variables.

When nuclear relaxation is much faster than exciton transport, it is possible to follow the dynamics of the exciton density matrix $N_{\alpha\beta}(t)$ (see Sec. IV) where all vibrational degrees of freedom are traced out. This level of reduction will be used in this paper. When nuclear dynamics is not fast, it is possible to identify a set of relevant collective vibrational variables that together with the excitonic variables are treated explicitly. A procedure for constructing the relevant slow collective variables based on the spectral densities of the system-bath coupling is described in Ref. 25. This treatment, however, goes beyond the scope of the present paper.

Exciton transport can be probed by a variety of nonlinear spectroscopic techniques, such as pump–probe[12–14,26,27] and three-pulse echo.[17–19] In this article we calculate the time- and frequency-gated fluorescence (TFGF)[28,29] (which is a linear incoherent technique) from molecular aggregates using the Doorway–Window (DW) representation. The DW picture in Liouville space, first developed by Yan and Mukamel for describing the nuclear density matrix for vibrations and the solvent,[30] offers an intuitive physical picture of the process. In this picture, the signal generation is described as a three step process involving the preparation, propagation, and detection of a wavepacket representing the exciton density matrix. First, the system interacts twice with the pump pulse, creating the Doorway wavepacket, that subsequently in the second step evolves during the time delay between the pump and the detection. In the third step, the Window wavepacket is created by the spontaneously emitted photon together with the gating device, and the signal is finally computed as the overlap of these two wavepackets in Liouville space. The DW representation for the pump–probe signal[31,32] which is very similar to the DW representation for the TFGF is discussed elsewhere.[33] The pump pulse and gating device are described using Wigner spectrograms, utilizing a mixed temporal and spectral representation of nonlinear spectroscopy developed in Ref. 34. Wigner spectrograms account for arbitrary pulse shapes and durations and interpolate naturally between the impulsive (time-resolved) and the ideal frequency-resolved limits.

This paper is organized as follows. In Sec. II we introduce the aggregate Hamiltonian described as a Frenkel-exciton system coupled to a harmonic bath, and discuss the linear absorption. In Sec. III we present the DW representation for the TFGF for an arbitrary Wigner spectrogram of the excitation pulse and arbitrary gating device. Details of the derivations based on Green function and projection operator techniques are given in Appendix A. In Sec. IV we introduce the Redfield equation for exciton transport.[35–39] Formal expressions for the Redfield relaxation superoperator for the exciton density matrix are given in Appendix B, and explicit expressions for this superoperator calculated using the Brownian oscillator spectral density are presented in Appen-

dix C. Numerical simulations are presented in Sec. V. Finally, we discuss the results and the connection with the master equation approach to transport in Sec. VI.

II. THE FRENKEL-EXCITON MODEL AND LINEAR ABSORPTION

Consider an aggregate made out of L interacting two-level chromophores. To describe its electronic states we introduce the exciton creation (annihilation) operators $\hat{B}_n^\dagger$ ($\hat{B}_n$) which add (eliminate) an excitation on the nth chromophore and satisfy the commutation relations[2,40]

$$[\hat{B}_m,\hat{B}_n^\dagger]=\delta_{mn}(1-2\hat{B}_n^\dagger\hat{B}_n). \tag{2.1}$$

Using these operators, the Frenkel Hamiltonian reads

$$H\equiv H_e+H_{\rm ph}+H_{\rm int}. \tag{2.2}$$

The first term represents the purely excitonic system:

$$H_e\equiv\sum_{mn} h_{mn}\hat{B}_m^\dagger\hat{B}_n, \tag{2.3}$$

where $h_{mn}\equiv\Omega_m\delta_{mn}+J_{mn}$, Ω_m is the exciton energy on the mth chromophore and J_{mn} is the exciton transfer matrix element.[2,3] H_e describes a tightly bound electron-hole pair (a Frenkel exciton) that moves coherently across the aggregate. It is a quasiparticle description that restricts the electron-hole pair to reside on the same molecule at all times and further prohibits two excitons from residing on the same molecule. This Hamiltonian uses the Heitler–London approximation, i.e., terms that do not conserve the number of excitons have been neglected. This is justified since the exciton frequencies Ω_m are considerably higher than the couplings J_{mn}. Diagonalization of h_{mn} results in the one-exciton eigenstates $|\alpha\rangle$ and energies ε_α

$$|\alpha\rangle=\sum_m \varphi_\alpha(m)B_m^\dagger|0\rangle, \tag{2.4}$$

which satisfy the Schrödinger equation

$$\sum_n h_{mn}\varphi_\alpha(n)=\epsilon_\alpha\varphi_\alpha(m). \tag{2.5}$$

$H_{\rm ph}$ is the bath (phonon) Hamiltonian, representing harmonic nuclear motions.

$$H_{\rm ph}\equiv\sum_\nu\left(\frac{p_\nu^2}{2m_\nu}+\frac{m_\nu\omega_\nu^2q_\nu^2}{2}\right). \tag{2.6}$$

q_ν, p_ν, m_ν, and ω_ν is the coordinate, momentum, mass and frequency of the νth normal mode. To lowest (linear) order in nuclear coordinates q_ν, the system-bath interaction is given by

$$H_{\rm int}\equiv\sum_{\nu,n} q_\nu\overline{\Omega}_{n,\nu}\hat{B}_n^\dagger\hat{B}_n+\sum_{mn,\nu}^{m\neq n} q_\nu\overline{J}_{mn,\nu}\hat{B}_m^\dagger\hat{B}_n, \tag{2.7}$$

where $\overline{J}_{nm,\nu}$ and $\overline{\Omega}_{n,\nu}$ are the vibronic coupling constants. Equation (2.7) represents the most general linear coupling of an exciton system to a harmonic bath.

Using the following set of collective bath coordinates:

$$\overline{q}_{mn}\equiv\sum_\nu m_\nu\omega_\nu^2(\delta_{mn}\overline{\Omega}_{n,\nu}+\overline{J}_{mn,\nu})q_\nu, \tag{2.8}$$

we introduce the matrix of spectral densities defined as the Fourier transform of the linear response functions of the collective coordinates,[41,25]

$$C_{mn,kl}(\omega)=\frac{i}{2}\int_{-\infty}^{\infty}dt\exp(i\omega t)\langle[\overline{q}_{mn}(t),\overline{q}_{kl}(0)]\rangle. \tag{2.9}$$

This matrix represents the frequency-dependent distribution of coupling constants for the bath oscillators, and contains all relevant information about the bath influence on the electronic system. Its frequency profile characterizes the dissipation.

The total Hamiltonian representing the system coupled to the optical field $\mathcal{E}(t)$ is

$$H_T(t)\equiv H-\mathcal{E}(t)P, \tag{2.10}$$

where P is the polarization operator

$$P=\sum_n \mu_n(\hat{B}_n^\dagger+\hat{B}_n), \tag{2.11}$$

and μ_n is the transition dipole moment of the nth chromophore.

To compute the optical response, we first define the exciton Green function

$$G_{mn}(t)\equiv\theta(t)\langle\hat{B}_m(t)\hat{B}_n^\dagger(0)\rangle, \tag{2.12}$$

where $\hat{B}_m(t)$ are interaction-picture operators:

$$\hat{B}_m(t)\equiv e^{iHt}\hat{B}_m e^{-iHt}, \tag{2.13}$$

and $\langle\cdots\rangle$ denotes an equilibrium average.

When the phonon degrees of freedom are traced out, the Green function acquires a self-energy Γ and in the frequency domain it assumes the form

$$G(\omega)=\frac{1}{\omega-H_e+i\Gamma}, \tag{2.14}$$

with matrix elements

$$G_{mn}(\omega)=\sum_\alpha\frac{\varphi_\alpha(m)\varphi_\alpha(n)}{\omega-\epsilon_\alpha+i\Gamma_\alpha} \tag{2.15}$$

and

$$\Gamma_\alpha\equiv\Gamma_{\alpha\alpha}=\sum_{mn}\varphi_\alpha(m)\varphi_\alpha(n)\Gamma_{mn}. \tag{2.16}$$

The frequency domain function $G(\omega)$ is related to its time domain counterpart by

$$G(\omega)=-i\int_{-\infty}^{\infty}dt\exp(i\omega t)G(t). \tag{2.17}$$

An additional factor $(-i)$ compared to a standard Fourier transform in the rhs of Eq. (2.17) uses the convention of Ref. 32.

A closed expression for the exciton dephasing matrix Γ_{mn} which represents the effect of coupling with phonons,

calculated to second order in exciton–phonon coupling and using the Markov approximation is given in Eq. (B6).

The linear absorption spectrum can be expressed in terms of the Green function:

$$S_{\rm abs}(\omega)=i\sum_{mn}\mu_m\mu_n[G_{mn}(\omega)-G^{\dagger}_{nm}(\omega)], \tag{2.18}$$

which using the exciton representation gives

$$S_{\rm abs}(\omega)=\sum_{\alpha}\frac{2|\mu_\alpha|^2\Gamma_\alpha}{(\omega-\epsilon_\alpha)^2+\Gamma_\alpha^2}, \tag{2.19}$$

where $\mu_\alpha\equiv\Sigma_\alpha\varphi_\alpha(m)\mu_m$ is the transition dipole of the α'th exciton.

III. DOORWAY–WINDOW REPRESENTATION OF THE FLUORESCENCE SIGNAL

In fluorescence spectroscopy the aggregate is subjected to an optical field

$$\mathcal{E}(t)=\mathcal{E}_1(t)\exp(-i\bar{\omega}_1 t)+c.c., \tag{3.1}$$

where $\bar{\omega}_1$ is a carrier frequencies and $\mathcal{E}_1(t)$ is the pulse envelope centered at $t=0$.

The emitted light passes through two gating devices (a spectral and a time gate, centered around frequency ω and time τ, respectively). The TFGF signal can be represented in the form:

$$S_{fl}(\tau;\omega)=\int_{-\infty}^{\infty}d\tau'\int_{-\infty}^{\infty}d\tau''\,\Phi(\tau,\omega;\tau',\tau'')\langle\tilde{P}(\tau'')\tilde{P}(\tau')\rangle, \tag{3.2}$$

where $\tilde{P}(\tau)$ denotes the polarization operator P in the Heisenberg picture for the system driven by an optical field (see Appendix A for details). The function $\Phi(\tau,\omega;\tau',\tau'')$ describes the combined effect of the time and frequency gating devices and connects the correlation function $\langle\tilde{P}(\tau'')\tilde{P}(\tau')\rangle$ to the TFGF signal. It satisfies

$$\Phi(\tau,\omega;\tau'',\tau')=\Phi^*(\tau,\omega;\tau',\tau''). \tag{3.3}$$

We adopt the following model for the gating device which corresponds to one of the examples considered in Ref. 34:

$$\Phi(\tau,\omega;\tau',\tau'')=F(\tau-\tau',\tau-\tau'')\exp[i\omega(\tau'-\tau'')], \tag{3.4}$$

where $F(\tau',\tau'')$ satisfies the relation [Eq. (3.3)] and is finite only for $|\tau'|,|\tau''|<\triangle\tau$. The gating function Φ [Eq. (3.4)] represents the combined effect of a time gate with width $\triangle\tau$ centered at τ and a spectral gate with width $\triangle\omega\sim 2\pi(\triangle\tau)^{-1}$ centered at ω.

The function $F(\tau',\tau'')$ that describes the gating through Eqs. (3.2) and (3.4) (hereafter referred to as the gating function) can be conveniently expressed in terms of its left $F_L(\tau'',\omega)$, right $F_R(\tau',\omega)$ or Wigner $F_W(\tau_+,\omega)$ spectrograms:

$$F(\tau',\tau'')=\int_{-\infty}^{\infty}\frac{d\omega}{2\pi}\exp[-i\omega(\tau'-\tau'')]F_L(\tau'',\omega), \tag{3.5}$$

$$F(\tau',\tau'')=\int_{-\infty}^{\infty}\frac{d\omega}{2\pi}\exp[-i\omega(\tau'-\tau'')]F_R(\tau',\omega), \tag{3.6}$$

$$F(\tau',\tau'')=\int_{-\infty}^{\infty}\frac{d\omega}{2\pi}\exp[-i\omega(\tau'-\tau'')]F_W[(\tau'+\tau'')/2,\omega]. \tag{3.7}$$

The three types of spectrograms are represented by the Fourier transforms of the gating function $F(\tau',\tau'')$ with respect to $(\tau'-\tau'')$ keeping either τ'',τ' or $\tau_+\equiv(\tau'+\tau'')/2$ fixed, respectively. The Wigner spectrogram is real whereas the other two are complex. Any two of the three spectrograms can be expressed in terms of the third one, e.g.,

$$F_L(\tau'',\omega)=\int_{-\infty}^{\infty}dt\int_{-\infty}^{\infty}\frac{d\omega'}{2\pi}\exp[-i(\omega'-\omega)t]\times F_W(\tau''-t/2,\omega'), \tag{3.8}$$

$$F_R(\tau',\omega)=\int_{-\infty}^{\infty}dt\int_{-\infty}^{\infty}\frac{d\omega'}{2\pi}\exp[-i(\omega'-\omega)t]\times F_W(\tau'+t/2,\omega'). \tag{3.9}$$

The information on the excitation pulse relevant for the fluorescence signal calculated within the rotating-wave approximation (RWA) is contained in the correlation function of the field amplitudes:

$$I(\tau'-\tau'')\equiv\langle\mathcal{E}_1(\tau')\mathcal{E}_1^*(\tau'')\rangle. \tag{3.10}$$

Here $\langle\cdots\rangle$ denote an ensemble average over stochastic fluctuations of the field. We shall represent the field in terms of the spectrograms $I_L(\tau'',\omega)$, $I_R(\tau',\omega)$, and $I_W(\tau_+,\omega)$. These are related to the correlation function $I(\tau',\tau'')$ through Eqs. (3.5), (3.6), and (3.7) with F replaced by I and satisfy the relations Eqs. (3.8) and (3.9). In terms of the correlation function, the spectrograms are given by

$$I_R(\tau;\omega)=\int_{-\infty}^{\infty}dt\exp(i\omega t)I(\tau,\tau+t), \tag{3.11}$$

$$I_L(\tau';\omega)=\int_{-\infty}^{\infty}dt\exp(i\omega t)I(\tau'-t,\tau'), \tag{3.12}$$

$$I_W(\tau_+;\omega)=\int_{-\infty}^{\infty}dt\exp(i\omega t)I(\tau_+-t/2,\tau_++t/2). \tag{3.13}$$

Hereafter we assume that the pump and the gate are temporally well separated compared to the exciton dephasing time scale Γ^{-1}. We can then neglect the direct scattering (Raman) contribution to the signal.[34,42] In Appendix A we derive a closed Green function expression for the signal. Substituting Eq. (A5) and a similar expression for $S(\tau-t_3,\tau)$ into Eq. (3.2) we obtain the Doorway–Window (DW) representation for the TFGF signal

$$S_{fl}(\tau,\omega)=\sum_{mnkl}\int_0^{\infty}d\tau'\int_0^{\infty}dt_2\,\mathcal{W}_{nm}(\tau-\tau',\omega)\times G^{(N)}_{mn,kl}(t_2)\mathcal{D}_{kl}(\tau'-t_2,\bar{\omega}_1). \tag{3.14}$$

The Doorway function $\mathcal{D}_{kl}(\tau'-t_2,\bar{\omega}_1)$ is the one-exciton wavepacket created by the laser pulse. It is a Hermitian matrix represented in the form

$$\mathcal{D}_{kl}(\tau'-t_2,\bar{\omega}_1)=\mathcal{D}_{kl,L}(\tau'-t_2,\bar{\omega}_1)+\mathcal{D}_{kl,R}(\tau'-t_2,\bar{\omega}_1), \tag{3.15}$$

where the left $\mathcal{D}_{kl,L}$ and right $\mathcal{D}_{kl,R}$ components satisfy the relation

$$\mathcal{D}_L(\tau'-t_2,\bar{\omega}_1)=[\mathcal{D}_R(\tau'-t_2,\bar{\omega}_1)]^\dagger, \tag{3.16}$$

which guarantees the Hermiticity of the Doorway wavepacket.

The Green function

$$G^{(N)}_{mn,kl}(t_2)\equiv\theta(t_2)\langle\hat{B}_l(0)\hat{B}^\dagger_n(t_2)\hat{B}_m(t_2)\hat{B}^\dagger_k(0)\rangle, \tag{3.17}$$

describes the propagation of the Doorway wavepacket during the delay period t_2. This results in a wavepacket $N_{mn}(\tau')$ at time τ' that has the form

$$N_{mn}(\tau')=\sum_{kl}\int_0^\infty dt_2\, G^{(N)}_{mn,kl}(t_2)\mathcal{D}_{kl}(\tau'-t_2,\bar{\omega}_1). \tag{3.18}$$

The Window described by a matrix $\mathcal{W}_{mn}(\tau-\tau',\omega)$ converts the wavepacket $N_{mn}(\tau')$ to the signal $S_{fl}(\tau,\omega)$:

$$S_{fl}(\tau,\omega)=\int_{-\infty}^\infty d\tau'\,\mathrm{Tr}[\mathcal{W}^\dagger(\tau-\tau',\omega)N(\tau')]. \tag{3.19}$$

The matrix $\mathcal{W}$ is not necessarily Hermitian, however, it follows from Eq. (3.19) that due to the Hermiticity of the exciton wavepacket N, the anti-Hermitian component of $\mathcal{W}$ does not contribute to the signal. This implies that $\mathcal{W}$ can be always taken to be Hermitian. In Appendix A we obtain

$$\mathcal{W}_{mn}(\tau-\tau',\omega)=\mathcal{W}_{mn,L}(\tau-\tau',\omega)+\mathcal{W}_{mn,R}(\tau-\tau',\omega) \tag{3.20}$$

with

$$\mathcal{W}_L(\tau-\tau',\omega)=[\mathcal{W}_R(\tau-\tau',\omega)]^\dagger. \tag{3.21}$$

The left and the right components of the Doorway and Window functions can be expressed in terms of their snapshot limit counterparts $\mathcal{D}^0_{mn,\alpha}(t_1)$ and $\mathcal{W}^0_{mn,\alpha}(t_3)$ and the spectrograms F_α and I_α, with $\alpha=L,R$. The expressions have a similar form

$$\mathcal{D}_\alpha(\tau'-t_2,\bar{\omega}_1)=\int_0^\infty dt_1\int_{-\infty}^\infty\frac{d\omega_1}{2\pi}\mathcal{D}^0_\alpha(t_1)I_\alpha(\tau'-t_2,\bar{\omega}_1-\omega_1)\times\exp(is_\alpha\omega_1t_1), \tag{3.22}$$

$$\mathcal{W}_\alpha(\tau-\tau',\omega)=\int_0^\infty dt_3\int_{-\infty}^\infty\frac{d\omega_3}{2\pi}\mathcal{W}^0_\alpha(t_3)F_\alpha(\tau-\tau',\omega_3-\omega)\times\exp(is_\alpha\omega_3t_3) \tag{3.23}$$

with $\alpha=L,R$ and $s_L=-s_R=1$.

The left and right components of the snapshot Doorway and Window functions that enter Eqs. (3.22) and (3.23) have the form

$$\mathcal{D}^0_{kl,L}(t_1)=\sum_p\mu_l\mu_pG_{kp}(t_1),\qquad \mathcal{D}^0_{kl,R}(t_1)=-\sum_p\mu_k\mu_pG^\dagger_{pl}(t_1), \tag{3.24}$$

$$\mathcal{W}^0_{mn,L}(t_3)=\sum_p G_{pn}(t_3)\mu_p\mu_m,\qquad \mathcal{W}^0_{mn,R}(t_3)=-\sum_p G^\dagger_{mp}(t_3)\mu_p\mu_n. \tag{3.25}$$

Equation (3.14) represents the signal in terms of the preparation, propagation and detection of the exciton wavepacket. The snapshot limit[34] can be obtained by formally setting

$$I_\alpha(\tau'-t_2,\omega_1-\bar{\omega}_1)=\delta(\tau'-t_2)\,\delta(\omega_1-\bar{\omega}_1), \tag{3.26}$$

$$F_\alpha(\tau-\tau',\omega_3-\omega)=\delta(\tau-\tau')\,\delta(\omega_3-\omega). \tag{3.27}$$

Four out of the six time integrations involved in calculating Eq. (3.14) can then be carried out immediately and the signal becomes

$$S^0_{fl}(\omega,\tau;\bar{\omega}_1)=\mathrm{Re}\sum_{mnkl}\mathcal{W}^0_{mn}(\omega)G^{(N)}_{mn,kl}(\tau)\mathcal{D}^0_{kl}(\bar{\omega}_1), \tag{3.28}$$

where $\mathcal{D}^0_{kl}(\bar{\omega}_1)$ and $\mathcal{W}^0_{mn}(\omega)$ are the Fourier transforms of $\mathcal{D}^0_{kl}(t_1)$ and $\mathcal{W}^0_{mn}(t)$:

$$\mathcal{D}^0_{kl}(\bar{\omega}_1)\equiv\int_{-\infty}^\infty dt_1\,e^{i\bar{\omega}_1t_1}\mathcal{D}^0_{kl}(t_1), \tag{3.29}$$

$$\mathcal{W}^0_{mn}(\omega)\equiv\int_{-\infty}^\infty dt\,e^{i\omega t}\mathcal{W}^0_{mn}(t). \tag{3.30}$$

We note the following limiting cases. Integrating Eq. (3.28) over ω, we obtain the time resolved snapshot fluorescence signal

$$S^0_{fl}(\tau,\bar{\omega}_1)=\mathrm{Re}\sum_{mnkl}\mu_m\mu_nG^{(N)}_{mn,kl}(\tau)\mathcal{D}^0_{kl}(\bar{\omega}_1), \tag{3.31}$$

whereas integration over τ gives the frequency-resolved signal

$$S^0_{fl}(\omega,\bar{\omega}_1)=\mathrm{Re}\sum_{mnkl}\int_{-\infty}^\infty d\tau\mathcal{W}^0_{mn}(\omega)G^{(N)}_{mn,kl}(\tau)\mathcal{D}^0_{kl}(\bar{\omega}_1). \tag{3.32}$$

Equation (3.14) is written in the local (chromophore) representation. For numerical applications it is preferable to recast it using the exciton $|\alpha\rangle$ representation. We then have

$$S_{fl}(\tau,\omega)=\sum_{\alpha\beta\gamma\delta}\int_0^\infty d\tau'\int_0^\infty dt_2\,\mathcal{W}_{\alpha\beta}(\tau-\tau',\omega)\times G^{(N)}_{\alpha\beta,\gamma\delta}(t_2)\mathcal{D}_{\gamma\delta}(\tau'-t_2,\bar{\omega}_1), \tag{3.33}$$

where

$$\mathcal{D}_{\gamma\delta}(\tau'-t_2,\bar{\omega}_1)\equiv\sum_{kl}\mathcal{D}_{kl}(\tau'-t_2,\bar{\omega}_1)\varphi_\gamma(k)\varphi_\delta(l), \tag{3.34}$$

$$\mathcal{W}_{\alpha\beta}(\tau-\tau',\omega)\equiv\sum_{mn}\mathcal{W}_{mn}(\tau-\tau',\omega)\varphi_\alpha(m)\varphi_\beta(n), \quad (3.35)$$

and

$$G^{(N)}_{\alpha\beta,\gamma\delta}(t_2)\equiv\sum_{mnkl}G^{(N)}_{mn,kl}(t_2)\varphi_\alpha(m)\varphi_\beta(n)\varphi_\gamma(k)\varphi_\delta(l). \quad (3.36)$$

This representation will be used in the following sections.

IV. REDFIELD EQUATIONS FOR EXCITON RELAXATION

Exciton transport enters the expressions for the fluorescence signal derived in Sec. III through the Green function $G^{(N)}_{\alpha\beta,\gamma\delta}$ describing the evolution of the reduced one-exciton density matrix

$$N_{\alpha\beta}(\tau)\equiv\sum_{mn}\varphi_\alpha(m)\varphi_\beta(n)\langle B^\dagger_m(\tau)B_n(\tau)\rangle. \quad (4.1)$$

The equations of motion for $N_{\alpha\beta}(\tau)$ obtained by eliminating the nuclear variables using projection operator techniques followed by the Markov approximation are known as the Redfield equations[35,36,38,39,41,43,44]

$$\frac{dN_{\alpha'\beta'}(t)}{dt}\equiv-i\omega_{\alpha'\beta'}N_{\alpha'\beta'}(t)-\sum_{\alpha\beta}\overline{R}_{\alpha'\beta',\alpha\beta}N_{\alpha\beta}(t), \quad (4.2)$$

where $\omega_{\alpha'\beta'}\equiv(\epsilon_{\alpha'}-\epsilon_{\beta'})$. Closed expressions for the complete Redfield relaxation superoperator $\overline{R}$ are given in Appendix B [Eqs. (B2) and (B3)]. The population block of $\overline{R}$ which connects the diagonal density matrix elements $N_{\alpha\alpha}$ and $N_{\alpha'\alpha'}$ satisfies the detailed balance

$$\frac{\overline{R}_{\alpha'\alpha',\alpha\alpha}}{\overline{R}_{\alpha\alpha,\alpha'\alpha'}}=\exp\left(-\frac{\omega_{\alpha'\alpha}}{kT}\right) \quad (4.3)$$

and

$$\overline{R}_{\alpha\alpha,\alpha\alpha}=-\sum_{\alpha'}^{\alpha\neq\alpha'}\overline{R}_{\alpha'\alpha',\alpha\alpha}. \quad (4.4)$$

These are necessary and sufficient conditions that ensure the conservation probability and that the excitons attain thermal equilibrium at long times.[32,45] The Green function $G^{(N)}_{\alpha\beta,\gamma\delta}$ is defined by the solution $N_{\alpha\beta}(t)$ to the Redfield equations

$$N_{\alpha\beta}(t)=\sum_{\gamma\delta}G^{(N)}_{\alpha\beta,\gamma\delta}(t)N_{\gamma\delta}(0). \quad (4.5)$$

It may be transformed from the exciton to the molecular basis

$$G^{(N)}_{mn,kl}(t)\equiv\sum_{\alpha\beta,\gamma\delta}\varphi_\alpha(m)\varphi_\beta(n)\varphi_\gamma(k)\varphi_\delta(l)G^{(N)}_{\alpha\beta,\gamma\delta}(t). \quad (4.6)$$

In the following calculations we adopt a more specific model for the spectral density. We assume that the coupling with phonons is diagonal, i.e., $\overline{q}_{mn}\neq0$ for $m=n$ only, that each molecule has its own bath, and the baths coupled to different molecules are uncorrelated and statistically identical. These yield[25]

$$C_{mn,kl}(\omega)=\delta_{mn}\delta_{kl}\delta_{mk}C(\omega). \quad (4.7)$$

We further use the Brownian oscillator spectral density for the phonon bath:[32]

$$C(\omega)=2\lambda\frac{\Lambda\omega}{\Lambda^2+\omega^2}. \quad (4.8)$$

Here Λ^{-1} is the nuclear relaxation time scale and λ is the exciton–phonon coupling strength. The complete Redfield superoperator for this model is given by Eqs. (C3)–(C5). Its population block assumes a particularly compact form and is presented in Eqs. (C6) and (C7). It should be noted that the Redfield theory is based on second order perturbation with respect to the exciton–bath coupling and the Markov approximation. It only holds for fast bath relaxation $\sqrt{2\lambda kT}\ll\Lambda,kT$. If this condition is not satisfied, the solution of the Redfield equation becomes unphysical and may even yield diagonal elements which are negative or larger than 1.

The Redfield relaxation superoperator simplifies considerably for high temperatures and fast bath relaxation which is the limiting case where the present theory applies. As shown in Appendix C, in this case we obtain

$$\overline{R}_{\alpha'\beta',\alpha\beta}=2\Delta^2\Lambda^{-1}(\delta_{\alpha'\alpha}\delta_{\beta'\beta}-\Psi_{\alpha'\beta'\alpha\beta}), \quad (4.9)$$

with $\Delta^2\equiv2\lambda kT$ and

$$\Psi_{\alpha\beta\gamma\delta}\equiv\sum_m\varphi_\alpha(m)\varphi_\beta(m)\varphi_\gamma(m)\varphi_\delta(m). \quad (4.10)$$

Equation (4.9) was first derived using a simple stochastic model proposed by Haken and Strobl.[38,39,46] It assumes that the site energies are given by uncorrelated Gaussian random variables with variance Δ^2 and fast correlation time Λ^{-1}. Alternatively, using the exciton basis, the Haken–Strobl model implies that the excitons encounter a succession of strong collisions whereby after each collision all exciton states are equally populated (irrespective of the initial state).[39] This shows that the Haken–Strobl model is an infinite-temperature approximation. The model applies, e.g., for triplet excitons which have a very weak coupling (narrow bandwidth) of a few cm^{-1} so that the infinite temperature $kT\gg$(bandwidth) is easily met. The Haken–Strobl model was recently applied for antenna complexes.[47,48] Note however that the ~600 cm^{-1} bandwidth in typical aggregates is higher than kT (~200 cm^{-1} for room temperature) so that the infinite temperature approximation does not hold and the general expressions [Eqs. (B2) and (B3)] that hold for all temperatures should be used instead of Eq. (4.9).

The issue of the exciton coherence size has drawn a considerable attention. We have shown that a precise and unambiguous definition may be given in terms of the inverse participation ratio of the exciton density matrix.[31] The density matrix for the propagated exciton wavepacket is

$$N_{mn}(\tau)\equiv\sum_{kl}\int_0^\infty dt_2\,G^{(N)}_{mn,kl}(t_2)\mathcal{D}_{kl}(\tau-t_2,\overline{\omega}_1), \quad (4.11)$$

and its inverse participation ratio is defined by[36]

$$P(\tau)=\left[L\sum_{mn}|N_{mn}(\tau)|^2\right]^{-1}\left[\left(\sum_{mn}|N_{mn}(\tau)|\right)^2\right] \quad (4.12)$$

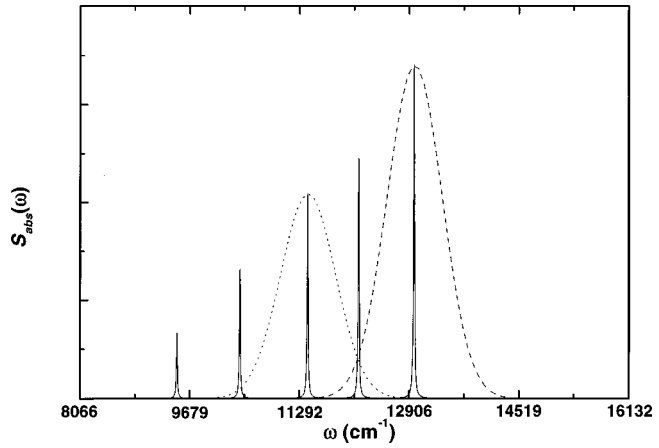

FIG. 1. The solid line shows the linear absorption spectrum [Eq. (2.19)] for the following model of pentamer aggregate. $\Omega_1=9679$, $\Omega_2=10\,486$, $\Omega_3=11\,292$, $\Omega_4=12\,099$, $\Omega_5=12\,906$, $J_{12}=403$, $J_{23}=484$, $J_{34}=323$, $J_{45}=242$. Other parameters are given in text. Power spectra of the pulse fields, $\bar{\omega}_1=12\,978$ (dashed line) and $\bar{\omega}_1=11\,413$ (dotted line). All frequencies are in cm^{-1}.

where L is the number of chromophores. The density matrix provides the proper averaged size relevant for optical signals such as fluorescence and superradiance.

V. NUMERICAL SIMULATIONS

We have calculated the TFGF signals and the exciton wavepacket dynamics for a linear aggregate consisting of five two-level chromophores. All chromophores have parallel transition dipoles and the same μ_n. Calculations were performed at room temperature $T=300$ K, exciton-bath coupling $\lambda=0.1$ cm^{-1}, and the inverse nuclear relaxation time, $\Lambda=50$ cm^{-1}. The linear absorption spectrum for this model is displayed in Fig. 1.

We assume the snapshot limit [Eq. (3.27)] for the gate and a Gaussian envelope of the pump

$$\mathcal{E}_1(t)=\exp\left(-\frac{t^2}{2\sigma^2}\right), \tag{5.1}$$

with $\sigma=15$ fs. Its Wigner spectrogram is

$$|I_W(t,\omega)|=\sqrt{4\pi\sigma^2}\exp\left(-\frac{t^2}{\sigma^2}-\sigma^2\omega^2\right). \tag{5.2}$$

In the first calculation we tuned, $\bar{\omega}_1=12\,978$ cm^{-1} to coincide with the highest exciton. The power spectrum of the pulse envelope

$$|\mathcal{E}(\omega)|^2\equiv\int dt\, I_W(t,\omega)=2\pi\sigma^2\exp(-\sigma^2\omega^2), \tag{5.3}$$

is shown by the dashed line in Fig. 1. The dispersed fluorescence signals [Eq. (3.33)] at various delay times are displayed in Fig 2. At $\tau=0$, the peak intensity from the highest exciton state is largest. At $\tau=5$ ns, all peak intensities become comparable and at $\tau=7$ ns, the lowest exciton peak starts to grow. In the long time limit, the propagated wavepacket relaxes towards the thermalized Boltzmann distribution of populations in the one-exciton manifold. At

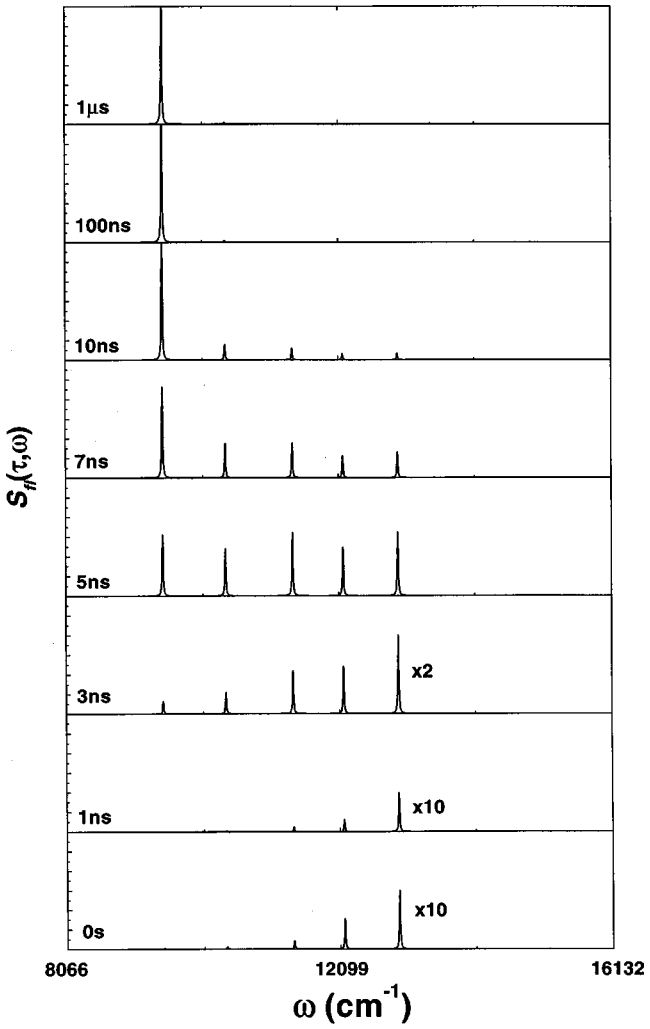

FIG. 2. Time and frequency resolved fluorescence signals for the model of Fig. 1. The pump carrier frequency is $\bar{\omega}_1=12\,978$ cm^{-1}.

$\tau=100$ ns, the system has reached thermal equilibrium. This is verified in Fig. 3 where we show the absolute values of the propagated density matrix exciton wavepacket,

$$|N_{\alpha\beta}(\tau)|\equiv\left|\sum_{\gamma\delta}\int_0^\infty dt_2\, G^{(N)}_{\alpha\beta,\gamma\delta}(t_2)\mathcal{D}_{\gamma\delta}(\tau-t_2,\bar{\omega}_1)\right|. \tag{5.4}$$

Coherences vanish at $\tau\cong 1$ ns and subsequently the populations evolve towards thermal equilibrium. We have repeated these calculations for $\bar{\omega}_1=11,413$ cm-1 (resonant with the middle exciton). The pump power spectrum is also shown in Fig. 1. The fluorescence spectra are shown in Fig. 4 and the absolute values of the propagated wavepackets are given in Fig. 5. In this case the emission from the initially pumped state is largest at $\tau=0$. The emission from higher exciton states decays as τ increases, whereas the peak from lowest state grows. The exciton system reaches thermal equilibrium at $\tau=100$ ns, as in Fig. 2.

VI. SUMMARY

We have derived a closed expression for the TFGF in the Doorway–Window representation, which provides an intuitive three-step picture: generation of the Doorway wave-

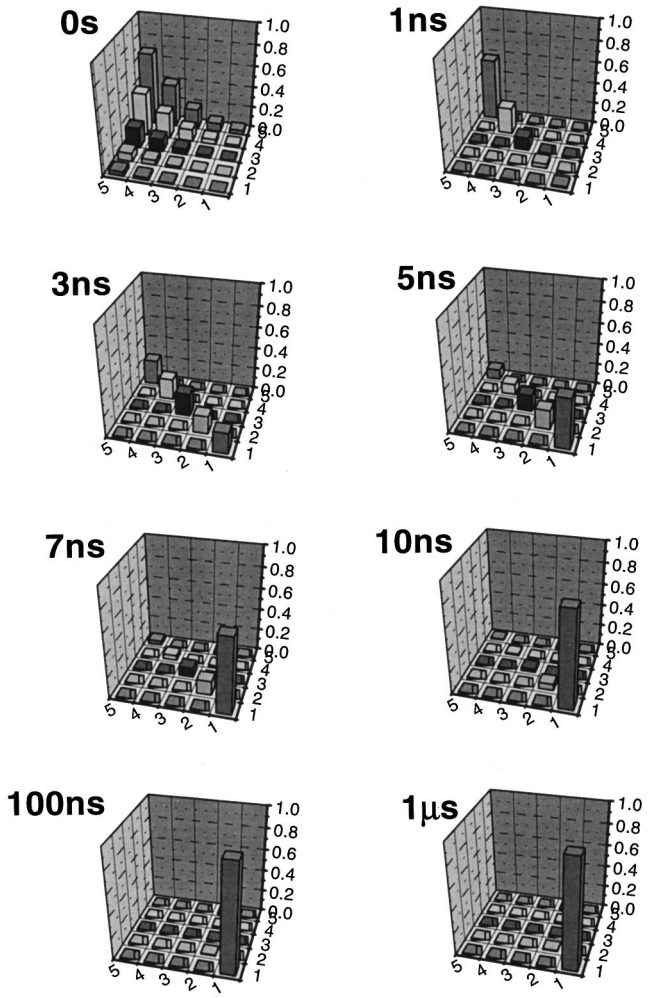

FIG. 3. Absolute values of propagated exciton wavepacket in the exciton basis [Eq. (5.4)] corresponding to Fig. 2.

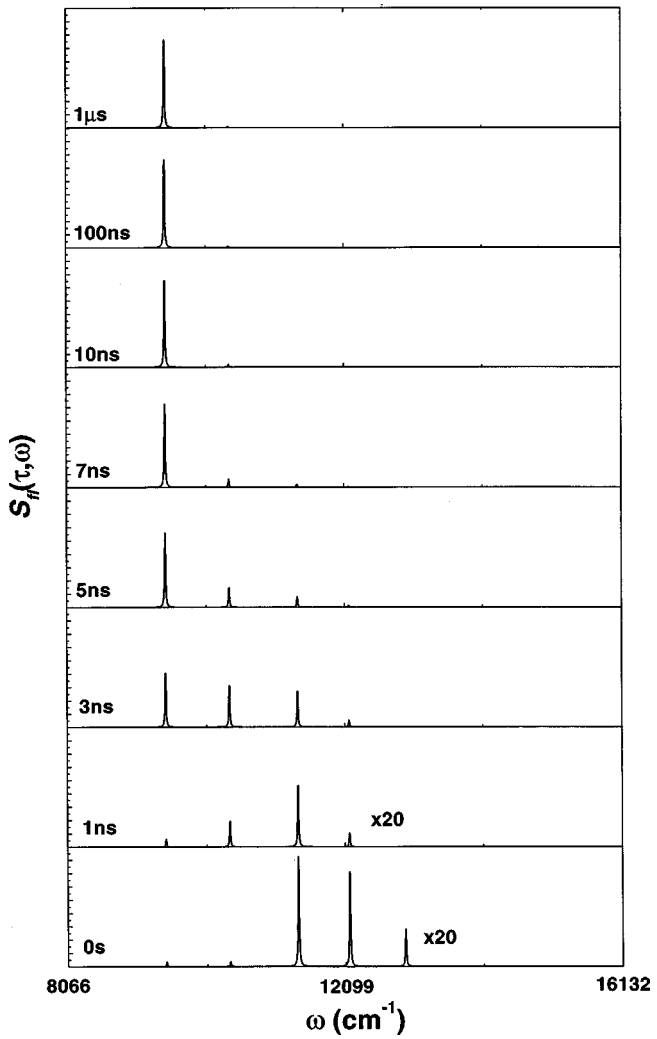

FIG. 4. Time and frequency fluorescence signals for the model of Fig. 1. The pump carrier frequency is $\bar{\omega}_1 = 11\,413\ \mathrm{cm}^{-1}$.

packet by the pump, relaxation of the wavepacket towards thermal equilibrium and detection of the signal by the overlap of the propagated wavepacket and the Window wavepacket. Wigner spectrograms for the excitation pulse and the gate account for arbitrary pulse shapes and durations and interpolate naturally between the time resolved and the frequency resolved limits. Relaxation of excitons is incorporated through the Green function $G^{(N)}$ calculated by solving the Redfield equations which describe the time evolution of the exciton density matrix N.

A simpler commonly used reduction scheme which only retains the populations, i.e., the diagonal elements of N is known as the master equation.[45,38,49] A notable advantage of the Redfield equation is that it can be easily transformed between basis sets, and the resulting exciton density matrix is invariant to such transformations; the choice of a basis set is immaterial. In contrast, since the term ''population'' is basis dependent, master equations derived for different choices of a basis set describe a different physical reality. In practice, two basis sets are often used, either the chromophore (molecular) or the exciton eigenstates. The master equation for chromophore populations N_{nn} may be adequate when the diagonal exciton–phonon coupling is strong compared to the intermolecular coupling. Strong exciton–phonon coupling causes dynamical localization of the excitations on the chromophores, and the coherences between different chromophores can be neglected. The rate in the corresponding master equation can be computed using the Forster–Dexter theory.[2,3]

When intermolecular coupling is strong compared to exciton–phonon coupling, we need to first diagonalize the Frenkel–exciton Hamiltonian and obtain the one-exciton eigenstates Eq. (2.5). The master equation for exciton populations $N_{\alpha\alpha}$ may be used when the system is small enough so that the distance between consecutive exciton levels is large compared to the phonon-induced exciton dephasing. Closed expressions for the master equations rate constants for the Brownian oscillator spectral density are given in Eqs. (C6) and (C7). Master equations do not usually apply for large aggregates: since the dephasing between the exciton states with close energies is weak, the coherences between such states may not be neglected, and the description in terms of exciton populations alone is not possible. One should rather retain explicitly all components of the density matrix and solve the Redfield equation. However, in some cases master

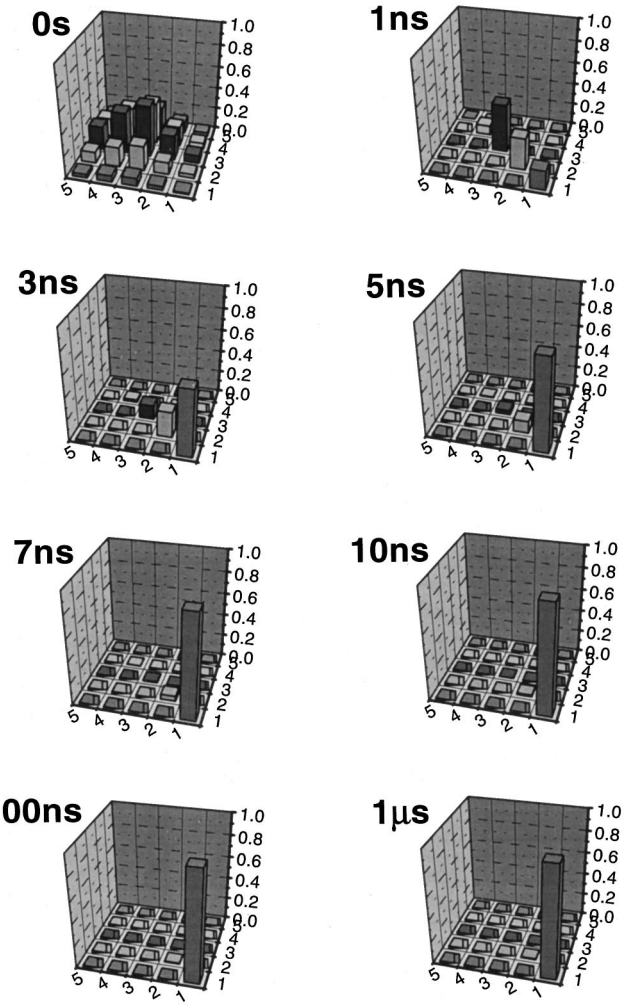

FIG. 5. Absolute values of propagated exciton wavepacket in the exciton basis [Eq. (5.4)], corresponding to Fig. 4.

equations may still be used even for large aggregates. For strong disorder the exciton states are localized and according to Mott,[50] states with close energies do not communicate and therefore do not interact by means of phonon exchange. This implies that there is an energy gap between communicating excitons, and the master equation can be used provided the exciton localization length is sufficiently short for the gap to exceed the dephasing rate.[51,52]

ACKNOWLEDGMENTS

We wish to thank Mats Dahlbom and Villy Sungstrom for useful discussions. The support of the National Science Foundation is gratefully acknowledged.

APPENDIX A: DOORWAY WINDOW REPRESENTATION FOR THE FLUORESCENCE SIGNAL

According to Eqs. (3.2) and (3.4), the TFGF signal can be expressed in terms of the gating function F and the correlation function $S(\tau',\tau'')$ of the polarization operator of the driven system

$$S(\tau',\tau'')\equiv\langle\tilde{P}(\tau'')\tilde{P}(\tau')\rangle, \tag{A1}$$

where $\tilde{P}$ stands for the Heisenberg picture operator. Expanding Eq. (A1) to first non-vanishing (i.e., second) order in the driving field, and retaining only those terms that survive the RWA yields[36,52]

$$\begin{aligned}S(\tau',\tau'')=\sum_{mnkl}\mu_m\mu_n\mu_k\mu_l\int_0^\infty dt'\int_0^\infty dt''\,I(\tau'-t',\tau''-t'')\\ \times\exp[-i\bar{\omega}_1(\tau'-t'-\tau''+t'')]\\ \times\langle\hat{B}_{lR}(\tau''-t'')\hat{B}^\dagger_{nR}(\tau'')\hat{B}_{mL}(\tau')\hat{B}^\dagger_{kL}(\tau'-t')\rangle,\end{aligned} \tag{A2}$$

where in the rhs of Eq. (A2) we have a four-point Liouville space correlation function of the free system (without the driving field). For an operator $\hat{A}$ we define the right and left superoperators as

$$\hat{A}_L(\hat{\rho})\equiv\hat{A}\hat{\rho},\quad \hat{A}_R(\hat{\rho})\equiv\hat{\rho}\hat{A}. \tag{A3}$$

In deriving Eq. (A2) we also made use of Eq. (2.11). The Liouville space correlation function can be evaluated using the projection operator technique developed in Ref. 51. To that end, we introduce the following projection operator $\mathcal{P}$

$$\mathcal{P}\rho\equiv\bar{\rho}_0\,\mathrm{Tr}_q(\rho), \tag{A4}$$

where Tr_q stands for the trace over vibrational degrees of freedom, $\bar{\rho}_0$ being the equilibrium vibrational density matrix in the ground electronic state, whereas ρ is a density matrix in the complete space.

We assume that the excitation pulse and the gating are temporarily well separated, i.e., their delay is large compared to the gating time window, the pulse duration, and the dephasing time Γ^{-1}. This implies that in Eq. (A2) $|\tau''-\tau'|,|t''-t'|\ll t'$. We then have four possible relative time orderings in the four-point correlation function in the rhs of Eq. (A2), defined by the signs of the time differences $(\tau''-\tau')$ and $(\tau''-t''-\tau'+t')$.

Introducing the consecutive time intervals $t_1,t_2,t_3\geqslant 0$ with $t_2\gg t_1,t_3$ we can recast Eq. (A2) in a form

$$\begin{aligned}S(\tau,\tau-t_3)=\sum_{mnkl}\mu_m\mu_n\mu_k\mu_l\int_0^\infty dt_2\int_0^\infty dt_1\{\mathrm{Tr}[\hat{B}_{mL}\mathcal{G}(t_3)\\ \times\hat{B}^\dagger_{nR}\mathcal{G}(t_2)\hat{B}_{lR}\mathcal{G}(t_1)\hat{B}^\dagger_{kL}\bar{\rho}]\\ \times I(\tau-t_3-t_2-t_1,\tau-t_3-t_2)\\ \times\exp(-i\bar{\omega}_1t_1)+\mathrm{Tr}[\hat{B}_{mL}\mathcal{G}(t_3)\hat{B}^\dagger_{nR}\mathcal{G}(t_2)\\ \times\hat{B}^\dagger_{kL}\mathcal{G}(t_1)\hat{B}_{lR}\bar{\rho}]I(\tau-t_3-t_2,\tau-t_3-t_2-t_1)\\ \times\exp(i\bar{\omega}_1t_1)\},\end{aligned} \tag{A5}$$

where $\mathcal{G}(t)\equiv\exp(-i\mathcal{L}t)$ with the Liouville operator $\mathcal{L}$.

One can obtain a similar expression for $S(\tau-t_3,\tau)$. It has been demonstrated[51] that if the bath relaxation time is fast compared to the exciton relaxation time scale, the Liou-

ville space evolution operator in Eq. (A5) can be replaced by $\mathcal{P}\mathcal{G}(t)\mathcal{P}$ with the projection operator $\mathcal{P}$ defined by Eq. (A4). This yields

$$\mathrm{Tr}[\hat{B}_{mL}\mathcal{G}(t_3)\hat{B}^{\dagger}_{nR}\mathcal{G}(t_2)\hat{B}_{lR}\mathcal{G}(t_1)\hat{B}^{\dagger}_{kL}\overline{\rho}] = \sum_{pq} G_{mp}(t_3)G^{(N)}_{pn,ql}(t_2)G_{qk}(t_1), \tag{A6}$$

$$\mathrm{Tr}[\hat{B}_{mL}\mathcal{G}(t_3)\hat{B}^{\dagger}_{nR}\mathcal{G}(t_2)\hat{B}^{\dagger}_{kL}\mathcal{G}(t_1)\hat{B}_{lR}\overline{\rho}] = -\sum_{pq} G_{mp}(t_3)G^{(N)}_{pn,kq}(t_2)G^{\dagger}_{lq}(t_1). \tag{A7}$$

Substituting Eqs. (A6) and (A7) in Eq. (A5), followed by substituting Eq. (A5) and a similar expression for $S(\tau-t_3,\tau)$ into Eq. (3.2) and making use of Eq. (A1) and Eq. (3.4) immediately yields the DW representation for the signal [Eq. (3.14)].[53]

APPENDIX B: THE REDFIELD RELAXATION SUPEROPERATOR

In this appendix we derive the Green function $G^{(N)}$ that propagates the Doorway wavepacket from its initial preparation stage to the final detection of a photon, during the time delay t_2. When the exciton–bath coupling is neglected, the density matrix satisfies the Liouville equation,

$$\frac{d}{dt}N_{mn}(t) = -i\sum_{m'}[H_{mm'}N_{m'n}(t) - N_{mm'}(t)H_{m'n}]. \tag{B1}$$

Using projection operator techniques and second order perturbation theory with respect to the exciton–bath coupling, we can take into account the effect of exciton–bath coupling on the time evolution of the density matrix in the one-exciton manifold.[41,36] The Redfield tensor for our model is then given by[41,36]

$$\overline{R}_{\alpha'\beta',\alpha\beta} = \int_0^{\infty} R_{\alpha'\beta',\alpha\beta}(t)\exp(i\omega_{\alpha\beta}t)dt, \tag{B2}$$

where $\omega_{\alpha\beta}\equiv\varepsilon_{\alpha}-\varepsilon_{\beta}$ and

$$\begin{aligned} R_{\alpha'\beta',\alpha\beta}(t) = &-\sum_{\gamma}\exp(i\omega_{\beta\gamma}t)M_{\alpha\gamma,\gamma\alpha'}(t)\delta_{\beta\beta'} \\ &+\exp(i\omega_{\beta\alpha'}t)M_{\alpha\alpha',\beta\beta'}(t) \\ &-\sum_{\gamma}\exp(i\omega_{\gamma\alpha}t)M^{*}_{\beta\gamma,\gamma\beta'}(t)\delta_{\alpha\alpha'} \\ &+\exp(i\omega_{\beta'\alpha}t)M^{*}_{\beta\beta',\alpha\alpha'}(t). \end{aligned} \tag{B3}$$

Using Eq. (2.9), we can write the spectral density in the time domain,[41]

$$\begin{aligned} M_{\alpha\beta,\gamma\delta}(t) = &\frac{1}{2}\int_{-\infty}^{\infty}\frac{d\omega}{2\pi}C_{\alpha\beta,\gamma\delta}(\omega) \\ &\times[\coth(\omega/2kT)\cos(\omega t) - i\sin(\omega t)], \end{aligned} \tag{B4}$$

where

$$C_{\alpha\beta,\gamma\delta}(\omega)\equiv\sum_{mn,kl}\varphi_{\alpha}(m)\varphi_{\beta}(n)\varphi_{\gamma}(k)\varphi_{\delta}(l)C_{mn,kl}(\omega), \tag{B5}$$

and $C_{mn,kl}(\omega)$ is given by Eq. (2.9).

Finally, the exciton dephasing matrix is given by[41]

$$\Gamma_{mn}\equiv -i\sum_{m'n'k}\int_0^{\infty}dt\,G^{0}_{m'n'}(t)M_{mm';n'k}(t)G^{0\dagger}_{kn}(t), \tag{B6}$$

with

$$G^{0}_{m'n'}(t)\equiv\theta(t)\langle m'|e^{-iH_e t}|n'\rangle. \tag{B7}$$

APPENDIX C: REDFIELD RELAXATION SUPEROPERATOR FOR THE BROWNIAN OSCILLATOR SPECTRAL DENSITY

Substituting the spectral density of a single strongly overdamped Brownian oscillator Eq. (4.8) into Eq. (B4) we obtain[54]

$$M_{\alpha\beta,\gamma\delta}(t) = \Psi_{\alpha\beta\gamma\delta}\mathcal{M}(t) \tag{C1}$$

and

$$\begin{aligned} \mathcal{M}(t) = \lambda\Lambda\Bigg[&\cot\left(\frac{\Lambda}{2kT}\right)\exp(-\Lambda t) + 4kT \\ &\times\sum_{n=1}^{\infty}\frac{\nu_n\exp(-\nu_n t)}{\nu_n^2-\Lambda^2} - i\exp(-\Lambda t)\Bigg], \end{aligned} \tag{C2}$$

where $\nu_n\equiv 2\pi nkT$ are the Matsubara frequencies.

Substituting this in Eqs. (B2) and (B3), the Redfield tensor is finally given by

$$\overline{R}_{\alpha'\beta',\alpha\beta} = R^{+}_{\alpha'\beta',\alpha\beta} + \overline{R}^{+}_{\alpha'\beta',\alpha\beta} + R^{-}_{\alpha'\beta',\alpha\beta} + \overline{R}^{-}_{\alpha'\beta',\alpha\beta}, \tag{C3}$$

where

$$\begin{aligned} R^{+}_{\alpha'\beta',\alpha\beta} = &-\lambda\Lambda\sum_{\gamma}\Psi_{\gamma\alpha\gamma\alpha'}\Bigg[\left(\cot\left(\frac{\Lambda}{2kT}\right)-i\right)\Upsilon_{\alpha\gamma}(\Lambda) \\ &+4kT\sum_{n=1}^{\infty}\frac{\nu_n}{\nu_n^2-\Lambda^2}\Upsilon_{\alpha\gamma}(\nu_n)\Bigg]\delta_{\beta\beta'}, \\ \overline{R}^{+}_{\alpha'\beta',\alpha\beta} = &\lambda\Lambda\Psi_{\alpha\beta\alpha'\beta'}\Bigg[\left(\cot\left(\frac{\Lambda}{2kT}\right)-i\right)\Upsilon_{\alpha\alpha'}(\Lambda) \\ &+4kT\sum_{n=1}^{\infty}\frac{\nu_n}{\nu_n^2-\Lambda^2}\Upsilon_{\alpha\alpha'}(\nu_n)\Bigg], \\ \overline{R}^{-}_{\alpha'\beta',\alpha\beta} = &\lambda\Lambda\Psi_{\alpha\beta\alpha'\beta'}\Bigg[\left(\cot\left(\frac{\Lambda}{2kT}\right)+i\right)\Upsilon_{\beta'\beta}(\Lambda) \\ &+4kT\sum_{n=1}^{\infty}\frac{\nu_n}{\nu_n^2-\Lambda^2}\Upsilon_{\beta'\beta}(\nu_n)\Bigg], \end{aligned} \tag{C4}$$

$$R^{-}_{\alpha'\beta',\alpha\beta}=-\lambda\Lambda\sum_{\gamma}\Psi_{\gamma\beta\gamma\beta'}\left[\left(\cot\left(\frac{\Lambda}{2kT}\right)+i\right)\Upsilon_{\gamma\beta}(\Lambda)+4kT\sum_{n=1}^{\infty}\frac{\nu_n}{\nu_n^2-\Lambda^2}\Upsilon_{\gamma\beta}(\nu_n)\right]\delta_{\alpha\alpha'}.$$

Here we have introduced the auxiliary function,

$$\Upsilon_{\alpha\beta}(Q)\equiv\frac{1}{Q-i\omega_{\alpha\beta}}. \tag{C5}$$

The population block of the Redfield tensor [Eq. (C3)] can be recast in a compact form

$$\begin{aligned}\overline{R}_{\alpha'\alpha',\alpha\alpha}=&-\lambda\Lambda\sum_{\gamma}\Psi_{\gamma\alpha\gamma\alpha'}\left[2\left\{\Lambda\cot\left(\frac{\Lambda}{2kT}\right)-\omega_{\alpha\gamma}\right\}\right.\\&\times\frac{1}{\Lambda^2+\omega_{\alpha\gamma}^2}+4kT\\&\left.\times\sum_{n=1}^{\infty}\frac{2\nu_n^2}{(\nu_n^2-\Lambda^2)(\nu_n^2+\omega_{\alpha\gamma}^2)}\right]\delta_{\alpha\alpha'}\\&+\lambda\Lambda\Psi_{\alpha\alpha\alpha'\alpha'}\left[2\left\{\Lambda\cot\left(\frac{\Lambda}{2kT}\right)-\omega_{\alpha\alpha'}\right\}\right.\\&\left.\times\frac{1}{\Lambda^2+\omega_{\alpha\alpha'}^2}+4kT\sum_{n=1}^{\infty}\frac{2\nu_n^2}{(\nu_n^2-\Lambda^2)(\nu_n^2+\omega_{\alpha\alpha'}^2)}\right]\end{aligned} \tag{C6}$$

and

$$\begin{aligned}\overline{R}_{\alpha\alpha,\alpha\alpha}=&-\lambda\Lambda\sum_{\gamma}\Psi_{\gamma\alpha\gamma\alpha}\left[2\left\{\Lambda\cot\left(\frac{\Lambda}{2kT}\right)-\omega_{\alpha\gamma}\right\}\right.\\&\left.\times\frac{1}{\Lambda^2+\omega_{\alpha\gamma}^2}+4kT\sum_{n=1}^{\infty}\frac{2\nu_n^2}{(\nu_n^2-\Lambda^2)(\nu_n^2+\omega_{\alpha\gamma}^2)}\right]\\&+\lambda\Lambda\Psi_{\alpha\alpha\alpha\alpha}\left[\frac{2}{\Lambda}\Lambda\cot\left(\frac{\Lambda}{2kT}\right)+4kT\right.\\&\left.\times\sum_{n=1}^{\infty}\frac{2}{(\nu_n^2-\Lambda^2)}\right].\end{aligned} \tag{C7}$$

At high temperatures the bath relaxation rate is determined by a typical oscillator frequency (Λ). The oscillators with frequencies higher than kT are frozen and do not contribute to the relaxation process. For $kT\ll\Lambda$ the relaxation is therefore dominated by the Matsubara rate $2\pi kT$. Our most general expressions for the Redfield superoperator [Eqs. (C3)–(C7)] hold when all bath timescales are fast $2\pi kT$, $\Lambda\gg\sqrt{2\lambda kT}$. These expressions are considerably simplified in the high-temperature limit $kT\gg\Lambda$. In Eq. (C4) we can then omit the sums over the Matsubara frequencies and replace the $\cot(\Lambda/2kT)$ factors by $2kT/\Lambda$. The Haken–Strobl limit is recovered when Λ is further large compared to the bandwidth (J). We can get $\Upsilon(\Lambda)=1/\Lambda$ and obtain

$$\begin{aligned}R^{+}_{\alpha'\beta',\alpha\beta}&=-\lambda\left(\frac{2kT}{\Lambda}-i\right)\delta_{\alpha\alpha'}\delta_{\beta\beta'},\\\overline{R}^{+}_{\alpha'\beta',\alpha\beta}&=\lambda\Psi_{\alpha\beta\alpha'\beta'}\left(\frac{2kT}{\Lambda}-i\right),\\\overline{R}^{-}_{\alpha'\beta',\alpha\beta}&=\lambda\Psi_{\alpha\beta\alpha'\beta'}\left(\frac{2kT}{\Lambda}+i\right),\\R^{-}_{\alpha'\beta',\alpha\beta}&=-\lambda\left(\frac{2kT}{\Lambda}+i\right)\delta_{\alpha\alpha'}\delta_{\beta\beta'}.\end{aligned} \tag{C8}$$

Substituting these in Eq. (C3) finally results in the Haken–Strobl superoperator [Eq. (4.9)].

[1] *J-aggregates*, edited by T. Kobayashi (World Scientific, Singapore, 1996).
[2] E. A. Silinish and V. Capek, *Organic Molecular Crystals* (American Institute of Physics, New York, 1994).
[3] M. Pope and C. E. Swenberg, *Electronic Processes in Organic Crystals* (Clarendon, New York, 1982).
[4] S. R. Forrest, Chem. Rev. **97**, 1793 (1997).
[5] A. Aziz, K. L. Narasimhan, N. Periasamy, and N. C. Maiti, Philos. Mag. B **79**, 993 (1999).
[6] E. I. Mal'tsev *et al.*, Appl. Phys. Lett. **73**, 3641 (1998).
[7] A. Gretchikhine, G. Schweitzer, M. van der Auweraer, R. de Keyzer, D. Vandenbroucke, and F. C. de Schryver, J. Appl. Phys. **85**, 1283 (1999).
[8] V. F. Kamalov, I. A. Struganova, and K. Yoshihara, Chem. Phys. Lett. **213**, 559 (1993).
[9] R. Gadonas, K.-H. Feller, and A. Pugzlys, Opt. Commun. **112**, 157 (1994); E. Gaizanskas, K.-H. Feller, and R. Gadonas, *ibid.* **118**, 360 (1995).
[10] K. Misawa, S. Machida, K. Horie, and T. Kobayashi, Chem. Phys. Lett. **240**, 210 (1995); T. Kobayashi, Mol. Cryst. Liq. Cryst. **283**, 17 (1996); K. Misawa and T. Kobayashi, Nonlinear Opt. **15**, 81 (1996).
[11] F. C. Spano, J. R. Kuklinski, and S. Mukamel, Phys. Rev. Lett. **65**, 211 (1990); J. Chem. Phys. **94**, 7534 (1991).
[12] V. Sundström, T. Pullerits, and R. van Grondelle, J. Phys. Chem. B **103**, 2327 (1999).
[13] V. Nagarajan, E. T. Johnson, J. C. Williams, and W. W. Parson, J. Phys. Chem. B **193**, 2297 (1999).
[14] D. C. Arnett, C. C. Moser, P. L. Dutton, and N. F. Scherer, J. Phys. Chem. B **103**, 2014 (1999).
[15] M. Rätsep, R. E. Blankenship, and G. J. Small, J. Phys. Chem. B **103**, 5736 (1999).
[16] J. Pieper *et al.*, J. Phys. Chem. A **103**, 2412 (1999); M. Rätsep *et al.*, J. Phys. Chem. B **102**, 4035 (1998).
[17] P. Schellenberg, R. J. W. Louwe, S. Shochat, P. Gast, and T. J. Aartsma, J. Phys. Chem. B **101**, 6786 (1997).
[18] R. J. W. Louwe and T. J. Aartsma, J. Phys. Chem. B **101**, 7221 (1997).
[19] R. Jimenez, R. van Mourik, J. Y. Yu, and G. R. Fleming, J. Phys. Chem. B **101**, 7350 (1997).
[20] R. van Grondelle, J. P. Dekker, T. Gillbro, and V. Sundström, Biochim. Biophys. Acta **1187**, 1 (1994).
[21] V. Sundström and R. van Grondelle, in *Anoxygenic Photosynthetic Bacteria*, edited by R. E. Blankenship, M. T. Madiga, and C. E. Baner (Kluwer Academic, Dordrecht, 1995), p. 349.
[22] R. Remelli, C. Varotto, D. Sandona, R. Croce, and R. Bassi, J. Biol. Chem. **274**, 33510 (1999); R. Simonetto, M. Crimi, D. Sandona, R. Croce, G. Cinque, J. Breton, and R. Bassi, Biochemistry **38**, 12974 (1999).
[23] M. R. Shortreed *et al.*, J. Phys. Chem. B **101**, 6318 (1997); C. Devadoss, P. Bharthi, and J. S. Moore, Macromolecules **31**, 8091 (1998).
[24] E. Y. Poliakov, V. Chernyak, S. Tretiak, and S. Mukamel, J. Chem. Phys. **110**, 8161 (1999); S. Tretiak, V. Chernyak, and S. Mukamel, J. Phys. Chem. B **102**, 3310 (1998).
[25] V. Chernyak and S. Mukamel, J. Chem. Phys. **105**, 4565 (1996).
[26] T. Pullerits, M. Chachisvilis, and V. Sundström, Chem. Phys Lett. **100**, 10787 (1996); T. Pullerits, M. Chachisvilis, M. R. Jones, C. N. Hunter,

and V. Sundström, Chem. Phys. Lett. **224**, 355 (1994).
[27] V. Nagarajan, R. G. Alden, J. C. Williams, and W. W. Parson, Proc. Natl. Acad. Sci. USA **93**, 13774 (1994).
[28] R. Jimenez, G. R. Fleming, P. V. Kumar, and M. Maroncelli, Nature (London) **369**, 471 (1994).
[29] H. Wang, J. Shah, T. C. Damen, and L. Pfeiffer, Phys. Rev. Lett. **74**, 3065 (1995); M. Woerner and J. Shah, *ibid.* **81**, 4208 (1998).
[30] Y. J. Yan and S. Mukamel, Phys. Rev. A **41**, 6485 (1990).
[31] T. Meier, V. Chernyak, and S. Mukamel, J. Phys. Chem. B **101**, 7332 (1997).
[32] S. Mukamel, *Principles of Nonlinear Optical Spectroscopy* (Oxford, New York, 1995).
[33] M. Dahlbom, V. Sundström, T. Minami, V. Chernyak, and S. Mukamel, J. Phys. Chem. (in press).
[34] S. Mukamel, C. Ciordas-Ciurdariu, and V. Khidekel, IEEE J. Quantum Electron. **32**, 1278 (1996); Adv. Chem. Phys. **101**, 345 (1997); S. Mukamel, J. Chem. Phys. **107**, 4165 (1997).
[35] A. G. Redfield, Adv. Magn. Reson. **1**, 1 (1965).
[36] W. T. Pollard, A. K. Felts, and R. A. Friesner, Adv. Chem. Phys. **93**, 77 (1997); W. T. Pollard and R. A. Friesner, J. Chem. Phys. **100**, 5054 (1994).
[37] A. Abragam, *The Principles of Nuclear Magnetism* (Oxford, London, 1961).
[38] V. W. Kenkre, *Exciton Dynamics in Molecular Crystals and Aggregates*, Springer Tracts in Modern Physics Vol. 94 (Springer, Berlin, 1982), p. 1; P. Reineker, *ibid.*, p. 111.
[39] J. Knoester and S. Mukamel, Phys. Rep. **205**, 1 (1991).
[40] W. M. Zhang, T. Meier, V. Chernyak, and S. Mukamel, J. Chem. Phys. **108**, 7763 (1998).
[41] V. Chernyak, W. M. Zhang, and S. Mukamel, J. Chem. Phys. **109**, 9587 (1998).
[42] S. Mukamel, Adv. Chem. Phys. **70**, 165 (1988).
[43] J. H. Eberly and K. Wodkiewicz, J. Opt. Soc. Am. **67**, 1252 (1977).
[44] J. M. Jean, J. Phys. Chem. A **102**, 7549 (1998).
[45] N. G. van Kampen, *Stochastic Processes in Physics and Chemistry* (North-Holland, Amsterdam, 1981).
[46] H. Haken and G. Strobl, Z. Phys. **262**, 135 (1973).
[47] J. A. Leegwater, J. Phys. Chem. **100**, 14403 (1996).
[48] S. I. E. Vulto *et al.*, J. Phys. Chem. B (in press).
[49] V. M. Axt, O. Kühn, and S. Mukamel, J. Lumin. **72–74**, 806 (1997).
[50] N. Mott, *Metal–Insulator Transition* (Taylor and Francis, London, 1974).
[51] T. Meier, V. Chernyak, and S. Mukamel, J. Chem. Phys. **107**, 8759 (1997).
[52] W. M. Zhang, T. Meier, V. Chernyak, and S. Mukamel, J. Chem. Phys. **108**, 7763 (1998).
[53] V. Chernyak, N. Wang, and S. Mukamel, Phys. Rep. **263**, 213 (1995).
[54] Y. Zhao, V. Chernyak, and S. Mukamel, J. Phys. Chem. A **102**, 6614 (1998).